Chapter 2
Towards High-Order Diffraction Suppression Using Two-Dimensional Quasi-Periodic Gratings

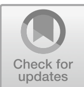

Changqing Xie, Lina Shi, Hailiang Li, Ziwei Liu, Tanchao Pu and Nan Gao

Abstract Two-dimensional (2D) diffraction gratings are playing an increasingly important role in the optics community due to their promising dispersion properties in two perpendicular directions. However, conventional 2D diffraction gratings often suffer from wavelength overlapping caused by high-order diffractions, and producing diffraction gratings with nanometer feature size still remains a challenge. In recent years, 2D quasi-periodic diffraction gratings have emerged that seek to suppress high-order diffractions, and to be compatibility with silicon planar process. This chapter reviews the optical properties of 2D quasi-periodic gratings comprised of quasi-triangle array of holes, and details the effects of hole shape and location distribution on the high-order diffraction suppression. It is also discuss the feasibility of various nanofabrication techniques for high volume manufacturing 2D quasi-periodic gratings at the nanoscale.

2.1 A Quick Tour of Diffraction Gratings

Diffraction gratings composed of periodic structures are simple and fundamental optical elements that separate incident light into its constituent wavelength components. The dispersive feature of diffraction gratings makes them attractive for fundamental studies and photonics applications in spectroscopy, microscopy, and interferometry [1–4]. Actually, since Joseph von Fraunhofer laid the foundation of diffraction gratings about 200 years ago, diffraction grating has been the most successful single optical device, and has found promising applications in widely diverse areas of physics, chemistry, biology, and engineering. For more details, one can see [5]. Among them, some related work on absorption and emission line spectroscopy investigations has been awarded Nobel Prizes [6].

C. Xie · L. Shi (✉) · H. Li · Z. Liu · T. Pu · N. Gao
Key Laboratory of Microelectronic Devices and Integrated Technology, Institute of Microelectronics, Chinese Academy of Sciences, Beijing 100029, People's Republic of China
e-mail: shilina@ime.ac.cn

© Springer Nature Switzerland AG 2019

P. Ribeiro et al. (eds.), *Optics, Photonics and Laser Technology 2017*,
Springer Series in Optical Sciences 222,
https://doi.org/10.1007/978-3-030-12692-6_2

2.1.1 Grating Equation

Various diffraction gratings with different configurations have been developed, they can be divided into two broad categories, reflection and transmission types [6, 7]. The former utilizes diffracted light on the same side of the grating normal, and can be further classified as plane and concave types. The latter utilizes diffracted light cross over the grating normal. The angle of diffraction measured from the grating normal can be quantitatively described by a simple expression, the well-known grating equation [6]

$$\sin\theta_m = (m\lambda - d\sin\theta_i)/d, \tag{2.1}$$

where d represents the grating period, λ is the incident light wavelength, θ_i denotes the angle between the incident light direction and the normal to the grating surface, and m is an integer known as the order of the diffracted light. Compared to the reflection gratings, transmission gratings are much simpler to use in monochromator and spectrometer. This is because they have higher figure error tolerances, smaller weight and size, wider bandwidth and easy-to-fabricate grating profiles, and greatly simplify the alignment at the expense of lower diffraction efficiency [8]. For most practical applications, only the generated +1st or −1st diffraction order is needed to realize the unique light dispersion. The resolving power R of a planar diffraction grating is the ability to separate and distinguish adjacent spectral lines in the constituent spectrum as a function of wavelength. It can be expressed as [6]

$$R = \lambda/\Delta\lambda = mN, \tag{2.2}$$

where N is the total number of grooves illuminated on the grating surface.

2.1.2 Overlapping of Diffraction Orders

Compared with a prism, one major disadvantage of planar diffraction gratings is that they suffer from higher-order diffraction contamination and limited free-spectral range due to the diffractive nature of planar periodic structures. When the bandwidth of the incident light is large enough, the grating equation can be fulfilled by an infinite set of wavelength values, i.e., light with wavelength λ in order m is always diffracted at the same angle as light with wavelength $\lambda/2$ in order $2m$, and as light of wavelength $\lambda/3$ in order $3m$, etc. The free spectral range is the bandwidth in a given order for which overlap of bandwidth from an adjacent order does not occur. It is equal to λ_1/m, where λ_1 is the short-wave end of the band, indicating that the free spectral range is longer for lower order. Actually, this is one reason that only the generated ±1st diffracted orders are needed in many applications.

2.1.3 *High Order Diffraction Suppression for 1D Gratings*

Traditionally, there are two possible ways to avoid the so-called overlapping of diffraction orders at a particular wavelength λ. One is to properly choose the planar grating period $D \in (\lambda, 2\lambda)$, which presents the major drawback of the wavelength range being limited to $(D, D/2)$. The other way is to use sinusoidal gratings with continuous relief [9]. However, the fabrication of continuous-relief diffractive optical elements is not compatible with the well-established silicon planar process, and still remains a challenge for mass production [10, 11].

Over the past decade, several methods have also been proposed to realize high order diffraction suppression for 1D gratings. In particular, Cao et al. proposed a binary grating composed of sinusoidal-shaped apertures to realize sinusoidal amplitude transmission at one direction [12]. After that, some new types of so-called single-order diffraction gratings, such as quantum-dot-array diffraction gratings [13], quasi-sinusoidal diffraction transmission gratings [14], modulated groove position diffraction gratings [15], zigzag diffraction transmission gratings [16], and trapezoidal transmission function [17], have been further developed. The key idea of all these work is to mimic a sinusoidal amplitude transmission function along one dimension by special structures. Single-order transmission diffraction gratings based on line-structure with rough edges [18] and dispersion engineered all-dielectric metasurfaces [19] have also been proposed. Besides, the order-sorting method using PbSe array detector [20] and thin films [21] have also been used to reduce the influence of higher-order diffractions.

2.2 Two-Dimensional Periodic Gratings

Thousands of papers have been published on various aspects of diffraction gratings, and most of them are devoted to 1D diffraction gratings consisting of a large number of equally spaced slits on an opaque screen. In recent years, two-dimensional (2D) diffraction gratings with complete order (periodic) structures have also received much attention due to their ability to simultaneously separate incident light into its constituent wavelength components in two perpendicular directions [22–27]. For example, in nearly all kinds of microscopes, 2D diffraction gratings are often used to calibrate the *xy*-plane [26]. In grating interferometry, 2D diffraction gratings are used to improve reconstruction of the wavefront phase [27].

Similar to the 1D case, 2D periodic structures also suffer from higher-order diffractions due to the diffractive nature of 2D structures. In order to get further insight into this, we begin our analysis from diffractions of a large number of identical and same oriented holes, as shown in Fig. 2.1. We denote the coordinate systems of the hole plane and the diffraction plane by (ξ, η) and (x, y), respectively. The coordinates of the hole center are (ξ_1, η_1), (ξ_2, η_2), …, (ξ_N, η_N). We calculate the far-field diffraction pattern of N holes with area A by Fraunhofer diffraction formula [9, 33]

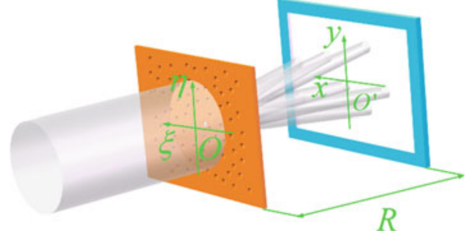

Fig. 2.1 Schematic of the 2D structures comprised of a large number of identical and same oriented holes

$$U(p,q) = C\sum_{n} e^{-ik(p\xi_n + q\eta_n)} \iint_A e^{-ik(p\xi' + q\eta')}\mathrm{d}\xi'\mathrm{d}\eta'. \tag{2.3}$$

Here $C = \sqrt{P}/(\lambda R)$, P is the power density incident on the hole array, R is the distance between the hole array plane and the observation plane, λ is the incident light wavelength, $k = 2\pi/\lambda$ is the wave vector in free space, and $p = x/R, q = y/R$.

From (2.3), the diffraction intensity pattern of a large number of holes in Fig. 2.1 can be expressed as

$$\begin{aligned} I(p,q) &= I^0(p,q) \cdot \left| \sum_{n=1}^{N} e^{-ik(p\xi_n + q\eta_n)} \right|^2 \\ &= I^0(p,q) \cdot \sum_{m=1}^{M}\sum_{n=1}^{N} e^{-ik[p(\xi_n - \xi_m) + q(\eta_n - \eta_m)]}, \end{aligned} \tag{2.4}$$

where $I^0(p,q)$ is the intensity distribution arising from a single hole and the remaining part denotes the interference effects of different holes. When we consider the effect of a large number of holes, we should obtain quite different results depending on whether the holes are distributed regularly or irregularly. When the holes are distributed irregularly, terms with different values of m and n will fluctuate rapidly between +1 and −1, and in consequence the sum of such terms will have zero mean value. Each remaining term ($m = n$) has the value unity. Hence the total intensity is N times the intensity of the light diffracted by a single hole: $I(p,q) \sim NI^0(p,q)$. The results are quite different when the holes are distributed regularly since the terms with $m \neq n$ will give appreciable contributions. For example, for some two dimensional array of holes, the phases of all the terms for which $m \neq n$ are exact multiple of 2π, their sum $I(p,q)$ will be equal to $N(N-1)$, and so for large N will be of the order of N^2.

Therefore, the locations of holes can be designed to create constructive interference leading to a subwavelength focus of prescribed size and shape [28–31]. The quasi-periodic distributed holes with special shape can acquire rich degrees of freedom (spatial position and geometric shape of holes) to realize complex functionalities, which are not achievable through periodic features of conventional grating with limited control in geometry. Thus, the suppression of high-order diffractions

can be realized by the destructive interference of light from quasi-periodic array with specific distribution and specific shape of the holes. At the same time, the 1st order diffraction efficiency can be increased by the constructive interference of lights from the different holes.

2.3 Two-Dimensional Quasi-Periodic Gratings

In this section, the effects of the quasi-periodic grating structure parameters on the diffraction property will be evaluated. From (2.3) and (2.4), the diffraction intensity pattern of the quasi-triangle array with periods P_ξ and P_η in Fig. 2.2 can be expressed as

$$\begin{aligned} I(p,q) &= \frac{\sin^2\left(N_\xi/2\cdot kp2P_\xi/2\right)\cdot\sin^2\left(N_\eta kqP_\eta/2\right)\cdot\cos^2\left(kp2P_\xi/4+kqP_\eta/4\right)}{\left(N_\xi/2\right)^2\cdot\sin^2\left(kp2P_\xi/2\right)\cdot N_\eta^2\cdot\sin^2\left(kqP_\eta/2\right)} \\ &\quad\cdot\left|C\iint\limits_A e^{ik(p\xi+q\eta)}\mathrm{d}\xi\,\mathrm{d}\eta\right|^2\cdot\left|\int\rho(s)\cdot e^{-ikps}\mathrm{d}s\right|^2 \\ &= I_1(p,q)\cdot I_2(p,q)\cdot I_3(p), \end{aligned} \tag{2.5}$$

where s is the hole location deviation from the triangle lattice point along ξ axis, the holes are randomly shifted by s according to probability distribution function $\rho(s)$. Here, the hole location along η axis is fixed since we usually focus on the diffraction property along one direction. And the triangle array is selected rather than square array due to the more spacing between any two adjacent holes than the square one with the same period and hole size. There are three parts in (2.4). The first part $I_1(p,q)=\frac{\sin^2\left(N_\xi/2\cdot kp2P_\xi/2\right)\cdot\sin^2\left(N_\eta kqP_\eta/2\right)\cdot\cos^2\left(kp2P_\xi/4+kqP_\eta/4\right)}{\left(N_\xi/2\right)^2\cdot\sin^2\left(kp2P_\xi/2\right)\cdot N_\eta^2\cdot\sin^2\left(kqP_\eta/2\right)}$, only depends on P_ξ, P_η, N_ξ and N_η. It is the interference effect resulting from the triangle array.

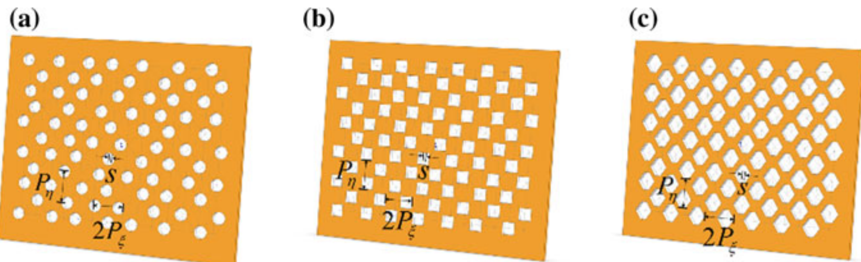

Fig. 2.2 Schematic of the quasi-triangle array gratings

The second part $I_2(p, q) = \left| C \iint_A e^{ik(p\xi + q\eta)} \mathrm{d}\xi \, \mathrm{d}\eta \right|^2$ denotes the effect of a single hole, and depends on the hole shape and size. It should be noted that the third part, $I_3(p) = \left| \int_S \rho(s) \cdot e^{-ikps} \mathrm{d}s \right|^2$, is introduced by the location deviation of holes. Equation (2.4) shows that the geometric shape and spatial position of holes can be optimized to manipulate the diffraction intensity pattern $I(p, q)$.

Next we investigate effects of the hole shape and size on the diffraction intensity pattern. Here we only consider some simple shapes with less sides since the complicated structures are difficult to be theoretically analyzed and precisely fabricated. We will discuss quasi-period gratings of circles, rectangles, and hexagons in Fig. 2.2.

2.3.1 Two-Dimensional Quasi-Triangle Array of Circular Holes

Firstly two-dimensional gratings of circular holes, which are the simplest will be discussed shape and easiest to be fabricated [32]. At the same time, the simplest uniform distribution of hole location will be selected. That is to say, the holes are shifted by s from the lattice points along the ξ axis according to the probability distribution $\rho(s) = 1/(2a)$, $|s| \leq a$, where a is the shift range of circle holes along the ξ axis. From (2.5), for the quasi-triangle array of $N_\xi N_\eta$ circular holes with the radius r, the diffraction intensity pattern in the Fraunhofer diffraction is given by

$$I(p, q) = \frac{\sin^2\left(N_\xi/2 \cdot kp2P_\xi/2\right) \cdot \sin^2\left(N_\eta kqP_\eta/2\right) \cdot \cos^2\left(kp2P_\xi/4 + kqP_\eta/4\right)}{\left(N_\xi/2\right)^2 \cdot \sin^2\left(kp2P_\xi/2\right) \cdot N_\eta^2 \cdot \sin^2\left(kqP_\eta/2\right)} \cdot I_0 \cdot \left[\frac{2J_1(kr\sqrt{p^2+q^2})}{kr\sqrt{p^2+q^2}}\right]^2 \cdot \mathrm{sinc}^2(kpa/\pi). \tag{2.6}$$

Here $I_0 = P/(\lambda R)^2 \cdot (N_\xi N_\eta \cdot \pi r^2)^2$ is the peak irradiance of the diffraction pattern and J_1 is the first order Bessel function of the first kind.

And the intensity along x axis is

$$I(p) = I_0 \cdot \left[\frac{\sin(kpP_\xi N_\xi/4)}{N_\xi \cdot \sin(kpP_\xi/4)}\right]^2 \cdot \left[\frac{2J_1(kpr)}{kpr}\right]^2 \cdot \mathrm{sinc}^2(kpa/\pi). \tag{2.7}$$

Equation (2.7) shows that the diffraction intensity along the x axis depends on the parameters of radius r and random range a. As described above, we can design r to make the first zero crossing of J_1 fall at some order diffraction such as the 2nd or 3rd order diffraction along x axis, and thus make it disappear. The third part $I_3(p) = \mathrm{sinc}^2(kpa/\pi)$, is introduced by the location deviation of holes. It should be noted that the normalized sinc has zero crossings occurring periodically at non-zero

integers. Thus we can optimize a to make these zero crossings of $\mathrm{sinc}^2(kpa/\pi)$ fall at even order diffractions.

Now we investigate the dependence of all order diffractions on the radius r and random range a. According to (2.7), the m-th order diffraction intensity along the ξ axis is

$$I(m) = I_0 \cdot \left[\frac{2J_1(2\pi mr/P_\xi)}{2\pi mr/P_\xi}\right]^2 \cdot \ \mathrm{sinc}^2(2ma/P_\xi). \tag{2.8}$$

In the real spectral measurement, only the adjacent diffractions (such as the 2nd and 3rd order diffractions) will overlap the 1st order diffraction. The higher order diffractions are usually very small and have little effects on the 1st order diffraction. Thus we pay the utmost attention to the structure parameters which lead to the vanishing of the 2nd and 3rd order diffractions. According to (2.8), the 2nd and 3rd order diffractions simultaneously disappear as $(r/P_\xi, a/P_\xi)$ take some special values: (0.203, 1/4), (0.305, 1/6), (0.305, 1/3), (0.372, 1/4). Considering the fabrication tolerance, we select $r/P_\xi = 0.203$ and $a/P_\xi = 0.25$ since the smallest spacing $\sqrt{(P_\xi - 2a)^2 + (P_\eta/2)^2} - 2r = 0.3011P_\xi$ (for $P_\xi = P_\eta$) of arbitrary adjacent holes is the largest one in the four cases of $(r/P_\xi, a/P_\xi)$. Here, it should be noted that the sinc function with $a/P_\xi = 0.25$ eliminates not only the 2nd order diffraction but also all the even order diffractions since it has periodic zero crossings.

Figure 2.3 presents the diffraction intensity pattern of $r/P_\xi = 0.203$ and $a/P_\xi = 0.25$ according to (2.6) and (2.7). As expected, Fig. 2.3a shows that the 0th and 1st order diffractions are kept along x axis, and high order diffractions disappear. Insets in Figs. 2.3b show clearly intensity distributions of the 0th and 1st order diffractions. The diffraction intensity along x axis in Fig. 2.3b presents clearly the complete suppression of the 2nd, 3rd 4th and 6th order diffractions. The 5th order diffraction of 5.370×10^{-5} is as low as 0.02% of the 1st order diffraction of 0.2637. As a result, it will be submerged in the background noise, i.e., it will decay to a negligible value in real experimental measurements.

In order to verify the validity of the theoretical analysis, the diffraction intensity pattern of the quasi-triangle array of 301×301 circular holes is simulated, according to (2.6) from Fraunhofer approximation. The locations of holes are determined by generating uniformly distributed pseudorandom numbers. The two-dimensional grating has the period. $P_\xi = P_\eta = 10\ \mu$m and the area 3.01 mm × 3.01 mm. Figure 2.4 shows that there exist the 0th and 1st order diffractions along x axis, and the 2nd, 3rd, 4th and 6th order diffractions disappear. Insets in Figs. 2.4b show clearly intensity distributions of the 0th and 1st order diffractions. The 5th order diffraction of 5.273×10^{-5} is as low as 0.02% of the 1st order diffraction of 0.2638. These agree very well with the theoretical results. Different from the theoretical results, the noise is introduced between any adjacent diffraction. Fortunately, the noise is much smaller than the 5th order diffraction and can be submerged in the background noise.

In order to further confirm the feasibility of the high order diffraction suppression of our theoretical predictions, a binary transmission grating comprised of quasi-

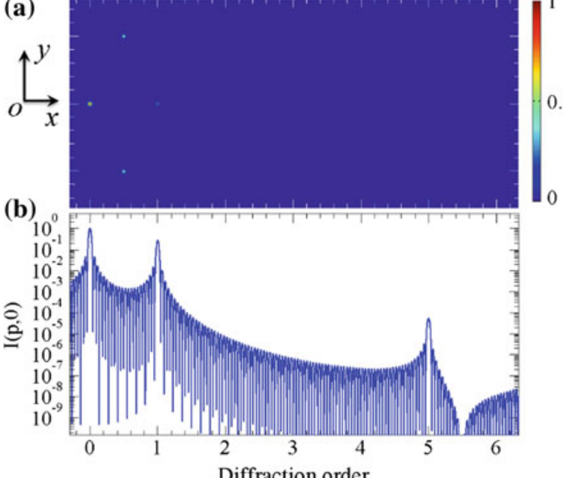

Fig. 2.3 **a** The far-field diffraction intensity pattern of the quasi-triangle array of circular holes. **b** The diffraction intensity along the *x* axis

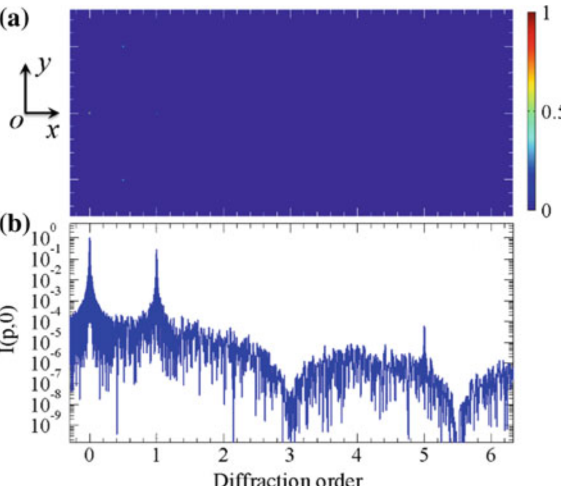

Fig. 2.4 **a** The far-field diffraction intensity pattern of the quasi-triangle array of 90,601 circular holes. **b** The diffraction intensity along the *x* axis

triangle array of 4000 × 4000 circular holes over area of 4 cm × 4 cm on a glass substrate was fabricated for the visible light region by laser write lithography. Firstly, the chromium layer with thickness of 110 nm was deposited onto the soda glass with 2.286 mm thickness with an electron beam evaporation system, and 500 nm thick AZ1500 photoresist was spin coated onto the chrome layer. Secondly, GDSII data of the designed binary gratings were imported into DESIGN WRITE LAZER 2000 (Heidelberg Instruments Mikrotechnik GmbH). Laser exposure and resist development were performed to pattern the binary gratings onto the resist. The exposure wavelength is 413 nm and the exposure power is 80 mW. After that, wet etching

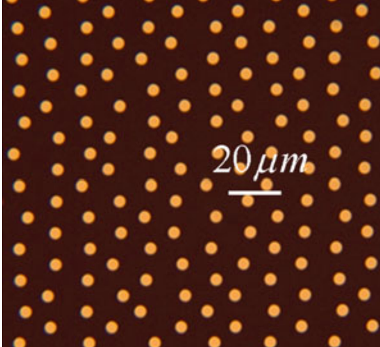

Fig. 2.5 Microphotograph of the fabricated quasi-triangle array of circular holes

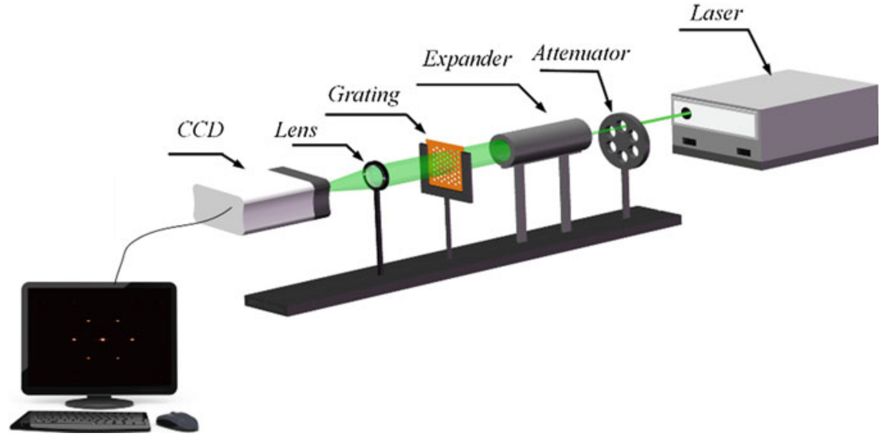

Fig. 2.6 .

technique was used to transfer the resist pattern onto the chrome layer. Finally, the residual resist was removed by using plasma ashing followed by acetone rinse.

The microphotograph of the fabricated structure is illustrated in Fig. 2.5. Periods $2P_\xi$ and P_η of the quasi-triangle array along the x and y axes are respectively 20 μm and 10 μm. The hole diameter is $0.406P_\xi \approx 4$ μm. It is shown clearly that the spacing between any two adjacent holes is larger than $0.3011P_\xi \approx 3$ μm. The experimental setup for optical demonstration is shown in Fig. 2.6. A collimated laser beams from Sprout (Lighthouse Photonics) with the wavelength of 532 nm was used to illuminate the two-dimensional grating, and the far-field diffraction pattern from the grating is focused by a lens and then recorded on a charge coupled device (CCD) camera (ANDOR DU920P-BU2) with 1024 × 256 pixels.

The measurement results were performed at low temperature of −85 °C, the results are shown in Fig. 2.7. It is clearly shown that only the 0th and the 1st orders exist along the x axis, which agrees well with the theoretical and simulation results.

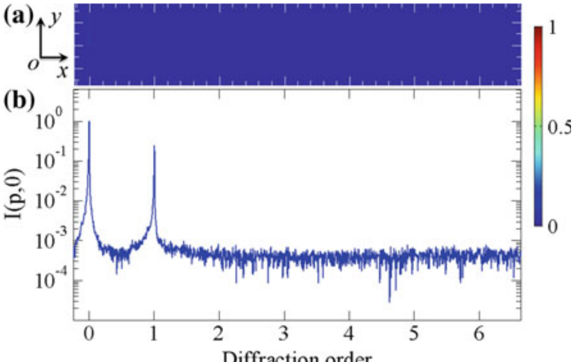

Fig. 2.7 **a** The far-field diffraction intensity pattern of the quasi-triangle array of circular holes. **b** The diffraction intensity along x axis

The 5th order diffraction (theoretical value 5.37×10^{-5}) cannot be observed, which is submerged in the background noise of 5×10^{-4}. The 1st order diffraction efficiencies is 23.99%, which is a little smaller than the theoretical value of 26.37%. The difference between experimental and theoretical values may be attributed to the fabrication and measurement errors.

In the above discussions, it has been assumed that the size and shape of holes are perfect. In practice, the size of fabricated holes can be a little larger or smaller than the designed target and the shape cannot be perfectly round. Thus the diffraction pattern will not be the same as the designed one. Numerical simulation based (2.5) is carried out and we obtain the 2nd, 3rd, 4th and 5th diffraction intensities versus the hole size in Fig. 2.8. The vertical grey dot line denotes the optimized diameter $2r = 4.0656\,\mu\text{m}$. Figure 2.8 shows that the 2nd and 4th order diffraction intensities are always zeros regardless of whether the hole diameter deviate the optimized value or not. This is because the disappearance of the even order diffractions result from zero crossings of the normalized sinc function, which is from the location randomness of holes. As $2r \in (3.6, 4.8)\,\mu\text{m}$, the 3rd order diffraction intensity will not be larger than 5×10^{-4}, even though it increases with the deviation of hole diameter from the optimized value. Similarly, the 5th order diffraction intensity is smaller than 3×10^{-4} as $2r \in (3.25, 4.9)\,\mu\text{m}$. Therefore, the quasi-periodic two-dimensional grating comprised of circular holes can, at least, tolerate $\pm 10\%$ deviation of hole size. This large tolerance makes our structure can be easily fabricated by the current planar silicon technology.

2.3.2 Two-Dimensional Quasi-Triangle Array of Rectangular Holes

Two-dimensional gratings of rectangular holes will now be discussed. The holes are shifted by s along the ξ axis (Fig. 2.2b) according to the probability distribution

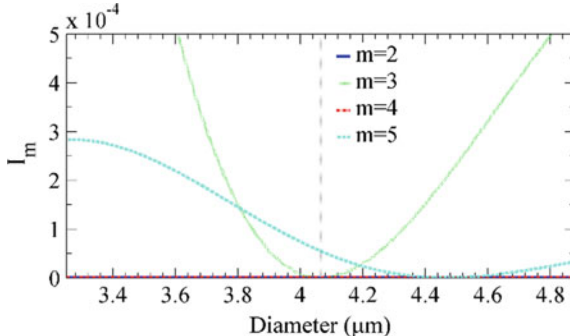

Fig. 2.8 The 2nd, 3rd, 4th and 5th order diffraction intensities versus the hole diameter

$\rho(s) = (\pi/P_\xi) \cdot \cos(2\pi s/P_\xi)$, $|s| \leq P_\xi/4$, where $2P_\xi$ is the period of the triangle array along the ξ axis [33].

For the quasi-triangle array of $N_\xi N_\eta$ rectangular holes of sides $2a = P_\xi/2$ and $2b = P_\eta/2$ as shown in Fig. 2.2b, the diffraction intensity pattern is [33]

$$I(p,q) = \frac{\sin^2\left(N_\xi/2 \cdot kp2P_\xi/2\right) \cdot \sin^2\left(N_\eta kqP_\eta/2\right) \cdot \cos^2\left(kp2P_\xi/4 + kqP_\eta/4\right)}{\left(N_\xi/2\right)^2 \cdot \sin^2\left(kp2P_\xi/2\right) \cdot N_\eta^2 \cdot \sin^2\left(kqP_\eta/2\right)} \cdot I_0 \cdot \left(\frac{\sin kpa}{kpa}\right)^2 \left(\frac{\sin kqb}{kqb}\right)^2 \cdot \frac{\cos^2(kpP_\xi/4)}{(1 - kpP_\xi/2/\pi)^2(1 + kpP_\xi/2/\pi)^2}. \quad (2.9)$$

Here $I_0 = P/(\lambda R)^2 \cdot (N_\xi N_\eta \cdot 4ab)^2$ is the peak irradiance of the diffraction pattern.

Figure 2.9 presents the diffraction intensity pattern according to (2.6). As expected, the 0th and 1st order diffractions are kept along x axis, and the high-order diffractions disappear. The logarithm of diffraction intensity along x axis in Fig. 2.9b presents clearly the complete suppression of the high order diffractions. Insets in Fig. 2.9 show the intensity distributions of the 0th and 1st order diffractions, respectively. From Fig. 2.9, one can see that the diffraction pattern of the quasi-triangle array of rectangular holes along x axis is the same as that of the ideal sinusoidal transmission grating.

Numerical simulation based on (2.9) is carried out to evaluate the diffraction property of the quasi-triangle array of 100,000 rectangular holes. The logarithm of diffraction intensity along x axis is shown in Fig. 2.10, and high-order diffraction is much less than the noise of 10^{-5} between 0th and 1st diffraction (red dash line in Fig. 2.10), which agrees well with the theoretical prediction of (2.9) and Fig. 2.9.

A binary transmission grating comprised of quasi-triangle array of rectangular holes was fabricated and tested by the above described process and setup. Figure 2.11 presents the recorded diffraction pattern and it is obvious that high order diffractions of the quasi-triangle array of rectangular holes are effectively suppressed. The diffraction intensity along x axis in Fig. 2.11b is almost the same as the ideal sinusoidal transmission gratings. The ratio of 1st order diffraction intensity to the 0th order diffraction intensity is 73.56% and much larger than the theoretical prediction and

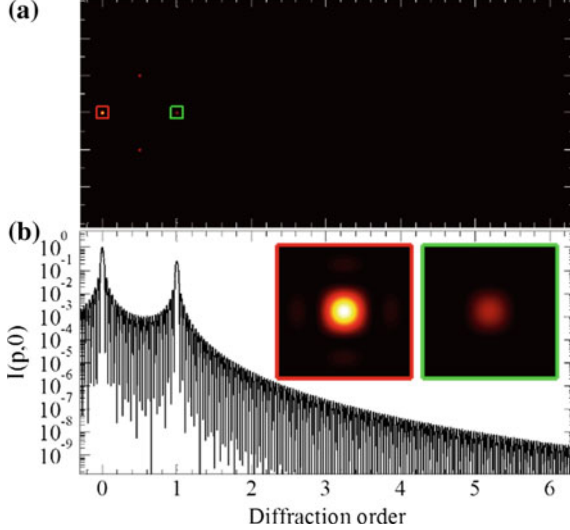

Fig. 2.9 The far-field diffraction intensity pattern of the quasi-triangle array of rectangular holes. **b** The diffraction intensity along *x* axis. Insets: the 0th and 1st order diffractions. (Reprinted from [33])

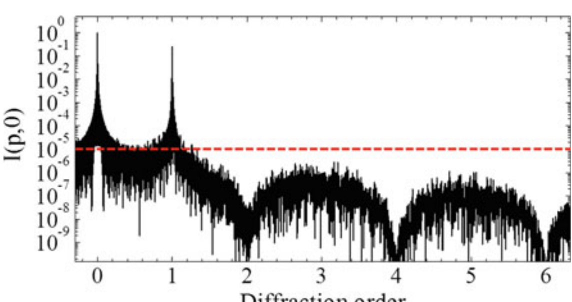

Fig. 2.10 The diffraction intensity along *x* axis of the quasi-triangle array with 100,000 rectangular holes. (Reprinted from [33])

numerical value 25%. This is because the CCD is saturated by the 0th order diffraction intensity. In addition, the red vertical lines in Fig. 2.11a are crosstalk along *y* direction due to our one-dimension CCD.

Now we focus on the complete suppression of high order diffractions along the *x* axis. As N_ξ is large enough, the intensity according to (2.9) along the *x* axis is given by [33]

$$I(p) = \frac{I_0 \cdot \mathrm{sinc}^2(N_\xi kp8a/\pi)}{(1 - kp2a/\pi)^2(1 + kp2a/\pi)^2\cos^2(kp4a)} = \begin{cases} I_0,\ p = 0 \\ \frac{1}{4}I_0,\ p = \frac{\pm\pi}{2ka} \end{cases} \tag{2.10}$$

Equation (2.10) demonstrates that the quasi-triangle array of infinite rectangular holes can generate the same diffraction pattern as sinusoidal transmission gratings along the *x* axis. Only three diffraction peaks (the 0th order and +1st/−1st orders)

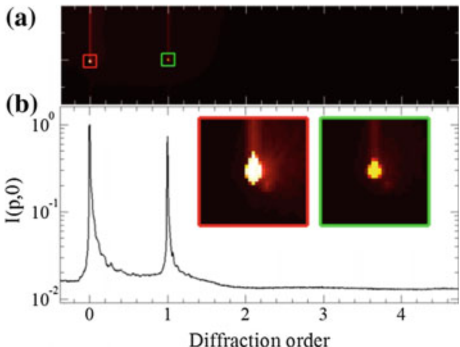

Fig. 2.11 **a** The far-field diffraction intensity pattern of the quasi-triangle array of rectangular holes. **b** The diffraction intensity along the ξ axis. (Reprinted from [33])

appear on the x-y plane. The above theoretical results are scalable from X-ray to far infrared wavelengths.

To obtain physical insight into the diffraction property of the quasi-triangle array of rectangular holes, the average transmission function along ξ axis is calculated by integrating the probability distribution over η axis [33]

$$T(\xi) = \int_{|\xi|-P_\xi/4}^{P_\xi/4} \rho(s)\mathrm{d}s = \frac{1}{2}(1 + \cos(\frac{2\pi}{P_\xi}\xi)). \tag{2.11}$$

Equation (2.11) shows that the quasi-triangle array of infinite rectangular holes has the same transmission function along the ξ axis as sinusoidal transmission gratings. It is the average diffractive effect similar to sinusoidal grating that eliminates high-order diffractions.

We can also understand the suppression of high-order diffractions by the interference weakening or strengthening. It is known that diffraction peaks is from the constructive interference of lights from the different holes. The interference of lights from different rectangular holes is controlled by the hole position. The desired diffraction pattern only containing the 0th order and +1st/−1st order diffractions can be tailored by the location distribution of holes according to some statistical law.

2.3.3 Two-Dimensional Quasi-Triangle Array of Hexagonal Holes

A grating with the quasi-triangle array of hexagonal holes to completely compressed the 2nd, 3rd, 4th, 5th and 6th order diffractions along x axis will now be addressed. The holes are shifted by s from the lattice points along the ξ axis according to the probability distribution $\rho(s) = 1/(2a)$, $|s| \leq a$, where a is the shift range of circle

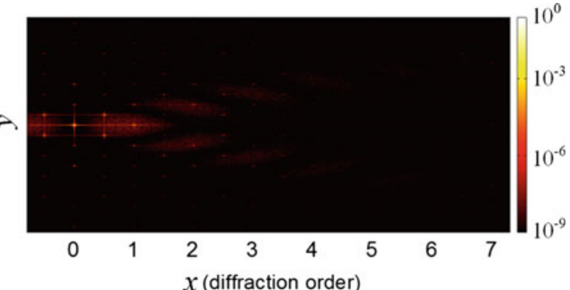

Fig. 2.12 The far-field diffraction intensity pattern of the quasi-triangle array of hexagonal holes

holes along the ξ axis. From (2.5), the diffraction intensity pattern $I(p, 0)$ can be described as

$$I(p,0) = \frac{\sin^2\left(N_\xi kpP_\xi/2\right)}{N_\xi^2 \cdot \sin^2\left(kpP_\xi/2\right)} \cdot \left(\frac{\sin(kp(a_2+a_1)/2)\cdot\sin(kp(a_2-a_1)/2)}{kp(a_2+a_1)/2\cdot kp(a_2-a_1)/2}\right)^2 \cdot \operatorname{sinc}^2(kpa/\pi). \tag{2.12}$$

Then the m-order diffraction intensity along x axis is

$$I(m) = \operatorname{sinc}^2\left(\frac{m(a_2+a_1)}{P_\xi}\right)\cdot\operatorname{sinc}^2\left(\frac{m(a_2-a_1)}{P_\xi}\right)\operatorname{sinc}^2\left(\frac{2ma}{P_\xi}\right). \tag{2.13}$$

Equation (2.13) shows that the m-order diffraction intensity $I(p, 0)$ is the product of three normalized sinc functions and depends on a, a_1 and a_2. Thus we can set $\frac{m(a_2+a_1)}{P_x} = n_1$, $\frac{m(a_2-a_1)}{P_x} = n_2$, and $\frac{2ma}{P_x} = n_3$ to suppress three kinds of the 2nd, 3rd, and 5th order diffractions.

In order to validate the theoretical analysis, numerical simulation for the case of $a = 1/10$, $a_1 = 1/12$ and $a_2 = 5/12$, has the lowest noise due to the smallest a. is carried out to evaluate the diffraction property of the quasi-triangle array with 100×100 hexagonal holes. As expected, the distribution of the diffraction intensity shown in Fig. 2.12 only has the 0th and ±1st order diffractions along x axis, and the 2nd, 3rd, 4th, 5th and 6th order diffractions are completely suppressed. Different from the theoretical results, the noise is introduced due to the shift of the hole position. The 7th order diffraction of 7.473×10^{-6} is almost submerged in the noise, and as low as 0.003% of the 1st order diffraction of 0.2426.

A binary transmission grating comprised of hexagonal holes was fabricated and tested by the above described process and setup. The diffraction property is shown in Fig. 2.13. The 2nd, 3rd, 4th, 5th and 6th order diffractions disappear along x axis. This quantitatively agrees with the theoretical and simulation results. The 1st order diffraction efficiency is 24.65%, which is a little different from the theoretical value of 24.26%. The difference may result from the fabrication and measurement errors.

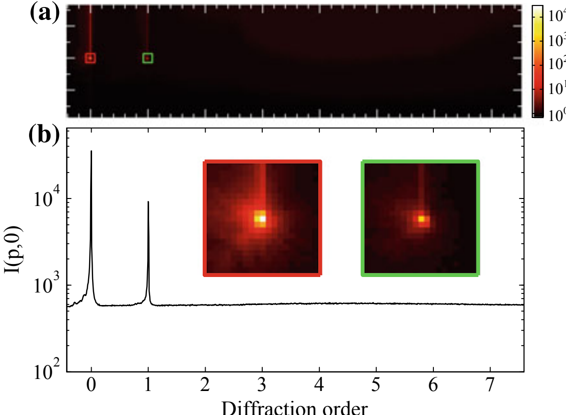

Fig. 2.13 The far-field diffraction intensity pattern of the quasi-triangle array with hexagonal holes. **b** The diffraction intensity along the x axis

As expected, Fig. 2.13 also shows that the 7th order diffraction is submerged in background noise.

2.3.4 Comparison of Three Types of Gratings

Table 2.1, summarizes the second part $I_2(p, 0)$ and $I_3(p)$ of (2.3), $I_2(p, 0)$ is the envelope line of the diffraction intensity pattern [9] and $I_3(p)$ is introduced by the location deviation of holes. $I_2(p, 0)$ only depends on one structure parameter for circular or rectangular holes, which can make the 2nd or even order diffractions zeros. Fortunately, for the hexagonal hole, $I_2(p, 0)$ is the product of two normalized sinc functions depending on the two parameters a_2 and a_1, and thus has two kinds of zero crossings, which can make both even and the 3rd, 6th, …, order diffractions simultaneously disappear.

In other words, three types have their advantages and disadvantages. Two-dimensional quasi-triangle array of circular holes the enough deviation tolerance of hole size and the relatively large spacing of adjacent holes, which make our grating much easy to be fabricated than the rectangular or hexagonal holes. While it only can completely suppress the 3rd and even order diffractions. The gratings composed of rectangular holes with the special location probability distribution can completely all the 2nd and higher order diffractions. However, the small gap from the probability distribution and the right angle of hole make the fabrication difficult. The hexagonal hole is the balance of the circular and rectangular holes. The complete suppression of 2nd, 3rd, 4th, 5th and 6th order diffractions by the quasi-triangle array of the hexagonal holes was demonstrated theoretically and experimentally. The 7th order diffraction is as low as 2.2×10^{-5} of the 1st order, which can easily be submerged in the background noise in real applications. At the same time, the smallest gap of

Table 2.1 The impact of the shape of the holes on the diffraction pattern

Shape	$I_2(p, 0)$	$\rho(s)$	$I_3(p)$
r	$\left(2J_1(krp)/krp\right)^2$	$1/(2a)$, $\lvert s\rvert \leq a$, $a = P_\xi/4$	$\mathrm{sinc}^2(kpa/\pi)$, $a = P_\xi/4$
$2b$ $2a_2$	$\mathrm{sinc}^2(kpa_2/\pi)$	$\rho(s) = (\pi/P_\xi)\cdot \cos(2\pi s/P_\xi), \lvert s\rvert \leq P_\xi/4$	$\frac{\cos^2(kpP_\xi/4)}{(1-kpP_\xi/2/\pi)^2(1+kpP_\xi/2/\pi)^2}$
$2a_1$ $2b$ $2a_2$	$\mathrm{sinc}^2(\frac{kp(a_2+a_1)}{2\pi})\cdot \mathrm{sinc}^2(\frac{kp(a_2-a_1)}{2\pi})$	$1/(2a)$, $\lvert s\rvert \leq a$, $a = P_\xi/10$	$\mathrm{sinc}^2(kpa/\pi)$, $a = P_\xi/10$

the hexagonal holes is larger than that of the rectangular gap, and thus the grating of hexagonal holes is easier to fabricate than the rectangular one.

2.4 Future Outlook for the Fabrication Method

Since the first diffraction grating was invented by the American astronomer David Rittenhouse in 1785 [6], great efforts have been devoted to the fabrication of high quality diffraction gratings [34, 35]. Until now, the difficulty in fabricating diffraction grating with nanometer feature size is still the major obstacle of advancing the dispersion performance. Various fabrication techniques, including mechanical ruling, interference lithography, e-beam lithography, laser beam lithography and nanoimprinting lithography, have been intensively studied to further reduce the feature size of diffraction grating.

2.4.1 The Mechanical Ruling Method

The first high quality diffraction grating was mechanically ruled [6]. After being polished carefully, the substrates (optical glass or fused silica) are coated with a thick aluminum or gold film. Such an Al or Au film acts as a functional material in the ruling process. Thousands of extremely fine and shallow grooves are faithfully produced by the ruling diamond with special shape in the cross section. For a ruled grating with 1000 grooves per mm and active area of $300 \times 300\ \mathrm{mm}^2$, the total groove number is 3.0×10^5, and the total length of these grooves is as large as 90 km. Thus, the ruling process is time consuming and the ultra-precision ruling engine may take

above one month to work. Now only a few ruling engine are still operating for planar echelle gratings greater than 300 mm in width [36, 37].

2.4.2 Interference Lithography

Since the invention of the laser in the 1960s, interference lithography has proven to be an extremely useful technique. The principle of traditional interference lithography is simple, when two mutually coherent plane waves with same wavelength and equal intensity interfere each other, sinusoidal interference fringes will be produced and recorded by photoresist on the substrate.

The spatial resolution of interference lithography is fundamentally governed by the working wavelength due to the diffraction limit. Hence, to produce gratings and grids with feature sizes below 100 nm, shorter working wavelengths (deep ultraviolet and extreme ultraviolet spectral ranges) are required [38]. Several interference lithography methods have been proposed and developed, including Lloyd's mirror interferometer [39], amplitude division interferometers [40], grating-based interference lithography [41], etc.

Interference lithography has the advantage of generating high resolution periodic patterns over large area with extremely simple optical systems, large process latitude and large depth-of-focus. Also, no photomask is needed, one can easily manipulate the grating period by adjusting the angle between the two intersecting beams. A typical example of successful use of interference lithography is provided by MIT space nanotechnology laboratory, where thousands of X-ray transmission gratings have been produced by interference lithography with wavelength of 351.1 nm [42]. By carefully selecting the number of interfering beam or multiple exposures, interference lithography can produce 2D periodic arrays with arbitrary shaped nanomotifs. However, interference lithography is limited to patterning period features only, and the spatial-period of the grating is fundamentally governed by the working wavelength due to the diffraction limit.

2.4.3 Electron Beam Lithography

Electron beam lithography is a well-established lithographic technique for creating arbitrarily shaped patterns with resolution in the nanometer range. At present, in semiconductor industry, electron beam lithography is often used to expose mask patterns for optical lithography tools below 45 nm technology node. In some cases, it is also used for advanced prototyping of integrated circuits due to its flexibility and high resolution.

For larger exposure latitude, the commercial e-beam writer acceleration voltage is taken to be 100 kV. The size of the focused electron beam, which is an important factor directly influencing the resolution, can be reduced to round 1 nm at the expense

of very low writing speed. Feature size below 5 nm is theoretically possible by exposing a thin (<30 nm) resist, but rarely demonstrated [43]. The actual patterning resolution is considerably larger and is limited mainly by the well-known proximity effect [44]. As charged particles, electrons undergo forward and backward scattering events when they penetrate through the resist into the substrate, resulting so-called proximity effect, i.e., unwanted dose to take place in the regions adjacent to those exposed by the focused electron beam.

Electron beam lithography is a promising approach for patterning 2D quasi-periodic gratings with high line density and high fidelity. In particular, it is convenient to perform pattern transfer from electron beam resist to a variety of materials. Obtaining high-quality grating patterns is always not straightforward, even using a state-of-the-art electron beam system. As a rule of thumb, for the 1D periodic gratings, the size of the focused electron beam can be one-sixth of the grating period for the purpose of higher writing speed. While for the 2D quasi-periodic gratings, this size should shrink to one-twelfth of the grating period to ensure sharp corners.

The drawback of the serial electron beam lithography is less practical in mass production due to the serial and slow scanning nature. To overcome this limitation, high-throughput multiple beam electron beam lithography, which is based on massively-parallel focused electron beams that can individually beam switched on and off, is now being developed.

2.4.4 Laser Beam Lithography

Laser beam lithography is performed by tightly focusing a laser beam instead of electron beam into a photoresist layer. Similar to serial electron beam lithography, the focused laser beam scans the patterned area to generate photoresist patterns pixel by pixel. On one hand, regarding the lithography costs, the less expensive laser beam lithography is now widely used for patterning mask above 45 nm technology node of semiconductor industry. On the other hand, it is also a powerful and widely used tool for the mask-free fabrication on various substrate materials.

Laser beam lithography is more flexible than the counterpart of electron beam lithography. For example, electron beam lithography must be performed on electrically conductive substrates with vacuum condition, while laser beam lithography is compatible with electrically insulating substrates and is performed under atmosphere condition. Furthermore, one-step laser beam lithography is capable of producing continuous-relief micro-structure with surface relief precision below 100 nm, which can be employed to increase the diffraction efficiency of the micro-optical elements.

In general, the spot size of the focused laser beam is fundamentally limited by the so-called Abbe's law, and is given by $\approx 1.22\ \lambda/\text{NA}$, where NA is the numerical aperture of the light exposure system. This constitutes a major fabrication challenge in achieving sub-diffraction or nanometer resolution at visible wavelengths. To overcome this limitation, in recent years, numerous method have reported on how the resolution of laser direct writing scales into nanometer dimension [45–48]. Remark-

ably, feature size as small as 9 nm has been achieved by three-dimensional optical beam lithography [48].

2.4.5 Nano-imprint Lithography

As stated above, the processes of mechanical ruling, electron beam lithography and laser beam lithography are serial and hence less practical in high-volume production, and interference lithography is limited to period structures.

Since the first paper was published by Chou et al. [49], nano-imprint lithography, a nanomolding technique to transfer the topography of a template into a substrate, has spurred extensive research by many academic groups. It is now considered as a candidate for next generation lithography by the International Technology Roadmap for Semiconductors (ITRS) roadmap [50, 51], due to its potential for simple, large-area, high-throughput, high-resolution patterning. It also offers a promising way to replicate master gratings.

In nano-imprint lithography, the first and the most important step is the fabrication of master gratings on silicon or quartz substrates. Typically, electron beam lithography or laser beam lithography is used to pattern master gratings due to its ability to generate arbitrary structure with fine features, followed by inductively coupled plasma reactive ion etching to transfer the resist patterns onto the substrate. Once the master grating is fabricated, it can be replicated repeatedly by nano-imprint lithography. The cost-effective imprinting can be performed by the thermal curing method, ultraviolet visible assisted method and injection moulding method, yielding a resist mask [52]. It should be noted that the template on a transparent substrate such as quartz or glass must be used for the ultraviolet visible assisted method, and the use of the transparent substrate make optical alignment of the substrate feasible. In addition, based on this ultraviolet visible transparent template, step and flash imprint lithography that performed at low pressure and room temperature has been developed at wafer-scale [53]. After imprinting, anisotropic oxygen plasma ashing is used to remove the residual thin resist layer. The resist pattern is further transferred into a hard material by lift-off process, electroplate process or plasma process.

2.5 Conclusion

In conclusion, the optics community has witnessed great progress over the past 200 years in the development of one-dimensional diffraction gratings. In recent years, two-dimensional diffraction gratings with two duty cycles in two perpendicular directions are playing an increasingly important role in the optics community. Most previous work on two-dimensional grating diffraction is for 2D periodic structures, which result in so-called high-order diffraction contamination and limited free-spectral range. To overcome this limitation, 2D quasi-periodic gratings com-

prised of quasi-triangle array of holes have been proposed, and the effects of hole shape (circular, rectangular and hexagonal) and location distribution on the high-order diffraction suppression have been investigated analytically, numerically, and experimentally. These three types of quasi-periodic diffraction gratings have been demonstrated to be robust in suppressing high-order diffractions, and have their advantages and disadvantages.

While the demand for diffraction gratings is widespread, producing a large supply of high quality diffraction gratings at low cost and high speed still remains a challenge. Even the best-established optical lithography can meet the stringent technical conditions of gradual reduction in the minimum dimension of integrated circuits, following the well-known Moore's law, it cannot be applied to produce diffraction gratings. This is because the optical lithography tool is very expensive. Mechanical ruling, interference lithography, electron beam lithography and laser beam lithography have been successfully used to fabricate diffraction gratings. However, interference lithography tool with high throughput and low cost is limited to period structures, and the other methods suffer from low yield. Advances in nano-imprint lithography have made possible the high-volume production of 2D quasi-periodic gratings with nanostructures. In nano-imprint lithography, electron beam lithography or laser beam lithography is used to exposure various predesigned patterns of master gratings in a maskless process, taking advantage of their high resolution and ability to create patterns of arbitrary geometry. The replication process of using imprinting lithography is used for high volume manufacturing of the daughter gratings, taking advantage of its high resolution, low cost, high speed, high process latitude and process robustness. The development of gratings nanofabrication process will allow the proposed quasi-periodic diffraction gratings to find a wide variety of applications in areas as diverse as spectral analysis, imaging and microscopy and interferometry.

Acknowledgements The authors are particularly grateful to the noteworthy assistance of their colleagues. We also would like to thank L. Cao for helpful discussion over many years. This work was funded by National Key Research and Development Program of China (2017YFA0206002) and National Natural Science Foundation of China (61275170, 61107032).

References

1. J. Strong, The Johns Hopkins University and diffraction gratings. J. Opt. Soc. Am. A **50**(12), 1148–1152 (1960)
2. R.L.C. Filho, M.G.P. Homem, R. Landers, A.N. de Brito, Advances on the Brazilian toroidal grating monochromator (TGM) beamline. J. Electron Spectrosc. Relat. Phenom. **144–147**, 1125–1127 (2005)
3. A. Freise, A. Bunkowski, R. Schnabel, Phase and alignment noise in grating interferometers. New J. Phys. **9**, 433 (2007)
4. H. Zhang, J. Zhu, Z. Zhu, Y. Jin, Q. Li, G. Jin, Surface-plasmon-enhanced GaN-LED based on a multilayered M-shaped nano-grating. Opt. Express **21**(11), 13492–13501 (2013)
5. C. Palmer, E. Loewen, in *Diffraction Grating Handbook* (Newport Corp., 2005)
6. http://web.mit.edu/spectroscopy/history/nobel.html

7. N. Bonod, J. Neauport, Diffraction gratings: from principles to applications in high-intensity lasers. Adv. Opt. Photonics **8**(1), 156–199 (2016)
8. R.K. Heilmann, M. Ahn, E.M. Gullikson, M.L. Schattenburg, Blazed high-efficiency x-ray diffraction via transmission through arrays of nanometer-scale mirrors. Opt. Express **16**, 8658–8669 (2008)
9. M. Born, E. Wolf, in *Principles of Optics* (Pergamon, London, 1980)
10. P. Jin, Y. Gao, T. Liu, X. Li, J. Tan, Resist shaping for replication of micro-optical elements with continuous relief in fused silica. Opt. Lett. **35**(8), 1169–1171 (2010)
11. G. Vincent, R. Haidar, S. Collin, N. Guérineau, J. Primot, E. Cambril, J.-L. Pelouard, Realization of sinusoidal transmittance with subwavelength metallic structures. J. Opt. Soc. Am. B **25**(5), 834–840 (2008)
12. L. Cao, E. Förster, A. Fuhrmann, C. Wang, L. Kuang, S. Liu, Y. Ding, Single order x-ray diffraction with binary sinusoidal transmission grating. Appl. Phys. Lett. **90**(5), 053501 (2007)
13. C. Wang, L. Kuang, Z. Wang, S. Liu, Y. Ding, L. Cao, E. Foerster, D. Wang, C. Xie, T. Ye, Characterization of the diffraction properties of quantum-dot-array diffraction grating. Rev. Sci. Instrum. **78**, 053503 (2007)
14. L. Kuang, L. Cao, X. Zhu, S. Wu, Z. Wang, C. Wang, S. Liu, S. Jiang, J. Yang, Y. Ding, C. Xie, J. Zheng, Quasi-sinusoidal single-order diffraction transmission grating used in x-ray spectroscopy. Opt. Lett. **36**(20), 3954–3956 (2011)
15. N. Gao, C. Xie, High-order diffraction suppression using modulated groove position gratings. Opt. Lett. **36**(21), 4251–4253 (2011)
16. H. Zang, C. Wang, Y. Gao, W. Zhou, L. Kuang, L. Wei, W. Fan, W. Zhang, Z. Zhao, L. Cao, Y. Gu, B. Zhang, G. Jiang, X. Zhu, C. Xie, Y. Zhao, M. Cui, Elimination of higher order diffraction using zigzag transmission grating in soft x-ray region. Appl. Phys. Lett. **100**(11), 111904 (2012)
17. Q. Fan, Y. Liu, C. Wang, Z. Yang, L. Wei, X. Zhu, C. Xie, Q. Zhang, F. Qian, Z. Yan, Y. Gu, W. Zhou, G. Jiang, L. Cao, Single-order diffraction grating designed by trapezoidal transmission function. Opt. Lett. **40**(11), 2657–2660 (2015)
18. F.J. Torcal-Milla, L.M. Sanchez-Brea, E. Bernabeu, Diffraction of gratings with rough edges. Opt. Express **16**(24), 19757–19769 (2008)
19. S. Gupta, Single-order transmission diffraction gratings based on dispersion engineered all-dielectric metasurfaces. J. Opt. Soc. Am. A **33**(8), 1641–1647 (2016)
20. W. Lee, H. Lee, J. Hahn, Correction of spectral deformation by second-order diffraction overlap in a mid-infrared range grating spectrometer using a PbSe array detector. Infrared Phys. Technol. **67**, 327–332 (2014)
21. F. Quinn, D. Teehan, M. MacDonald, S. Downes, P. Bailey, Higher-order suppression in diffraction-grating monochromators using thin films. J. Synchrotron Radiat. **5**, 783–785 (1998)
22. R. BrZuer, O. Bryngdahl, Electromagnetic diffraction analysis of two-dimensional gratings. Opt. Commun. **100**, 1–5 (1993)
23. E. Grann, M. Moharam, D.A. Pommet, Artificial uniaxial and biaxial dielectrics with use of two-dimensional subwavelength binary gratings. J. Opt. Soc. Am. A **11**(10), 2695–2703 (1994)
24. M. Kagias, Z. Wang, P. Villanueva-Perez, K. Jefimovs, M. Stampanoni, 2D-omnidirectional hard-x-ray scattering sensitivity in a single shot. Phys. Rev. Lett. **116**, 093902 (2016)
25. S. Rutishauser, M. Bednarzik, I. Zanette, T. Weitkamp, M. Borner, J. Mohr, C. David, Fabrication of two-dimensional hard X-ray diffraction gratings. Microelectron. Eng. **101**, 12–16 (2013)
26. G. Dai, F. Pohlenz, T. Dziomba, M. Xu, A. Diener, L. Koenders, H. Danzebrink, Accurate and traceable calibration of two-dimensional gratings. Meas. Sci. Technol. **18**, 415–421 (2007)
27. Y. Kayser, S. Rutishauser, T. Katayama, T. Kameshima, H. Ohashi, U. Flechsig, M. Yabashi, C. David, Shot-to-shot diagnostic of the longitudinal photon source position at the SPring-8 Angstrom Compact Free Electron Laser by means of x-ray grating interferometry. Opt. Lett. **41**(4), 733–736 (2016)
28. L. Kipp, M. Skibowski, R.L. Johnson, R. Berndt, R. Adelung, S. Harm, R. Seemann, Sharper images by focusing soft X-rays with photon sieves. Nature **414**(6860), 184–188 (2001)

29. K. Huang, H. Liu, F. J. Garcia-Vidal, M. Hong, B. Luk'yanchuk, J. Teng, C. Qiu, Ultrahigh-capacity non-periodic photon sieves operating in visible light. Nat. Commun. **6**, 7059 (2015)
30. C. Xie, X. Zhu, H. Li, L. Shi, Y. Hua, M. Liu, Toward two-dimensional nanometer resolution hard X-ray differential-interference-contrast imaging using modified photon sieves. Opt. Lett. **37**(4), 749–751 (2012)
31. F. Huang, T. Kao, V. Fedotov, Y. Chen, N. Zheludev, Nanohole array as a lens. Nano Lett. **8**(8), 2469–2472 (2008)
32. J. Niu, L. Shi, Z. Liu, T. Pu, H. Li, G. Wang, C. Xie, High order diffraction suppression by quasi-periodic two-dimensional gratings. Opt. Mater. Express **7**, 366–375 (2017)
33. L. Shi, H. Li, Z. Liu, T. Pu, N. Gao, C. Xie, The quasi-triangle array of rectangular holes with the completely suppression of high order diffractions, in *Proceedings of the 5th International Conference on Photonics, Optics and Laser Technology—Volume 1: PHOTOPTICS*, Porto, Portugal, 2017, pp. 54–58
34. E. Di Fabrizio, S. Cabrini, D. Cojoc, F. Romanato, L. Businaro, M. Altissimo, B. Kaulich, T. Wilhein, J. Susini, M. De Vittorio, E. Vitale, G. Gigli, R. Cingolani, Shaping X-rays by diffractive coded nano-optics. Microelectron. Eng. **67–68**, 87–95 (2003)
35. H.I. Smith, 100 years of x-ray: impact on micro- and nanofabrication. J. Vac. Sci. Technol. B, **13**, 2323–2328 (1995)
36. G.R. Harrison, S.W. Thompson, H. Kazukonis, J.R. Connell, 750-mm ruling engine producing large gratings and echelles. J. Opt. Soc. Am. **62**, 751–756 (1972)
37. X. Li, H. Yu, X. Qi, S. Feng, J. Cui, S. Zhang, J. Tu, Y. Tang, 300 mm ruling engine producing gratings and echelles under interferometric control in China. Appl. Opt. **54**, 1819–1826 (2015)
38. B. Paivanranta, A. Langner, E. Kirk, C. David, Y. Ekinci, Sub-10 nm patterning using EUV interference lithography. Nanotechnology **22**, 375302 (2011)
39. A. Ritucci, A. Reale, P. Zuppella, L. Reale, P. Tucceri, G. Tomassetti, P. Bettotti, L. Pavesi, Interference lithography by a soft x-ray laser beam: nanopatterning on photoresists. J. Appl. Phys. **102**(3), 034313–034314 (2007)
40. P. Wachulak, M. Grisham, S. Heinbuch, D. Martz, W. Rockward, D. Hill, J. Rocca, C. Menoni, E. Anderson, M. Marconi, Interferometric lithography with an amplitude division interferometer and a desktop extreme ultraviolet laser. J. Opt. Soc. Am. B **25**, 104–107 (2008)
41. H. Shiotani, S. Suzuki, D. Gun Lee, P. Naulleau, Y. Fukushima, R. Ohnishi, T. Watanabe, H. Kinoshita, Dual grating interferometric lithography for 22-nm node. Jpn. J. Appl. Phys. **47**, 4881–4885 (2008)
42. M.L. Schattenburg, C.R. Canizares, D. Dewey, K.A. Flanagan, M.A. Hamnett, A.M. Levine, K.S.K. Lum, R. Manikkalingam, T.H. Markert, H.I. Smith, Transmission grating spectroscopy and the Advanced X-Ray Astrophysics Facility (AXAF). Opt. Eng. **30**(10), 1590–1600 (1991)
43. J.K.W. Yang, B. Cord, H. Duan, K.K. Berggren, J. Klingfus, S.W. Nam, K.B. Kim, M.J. Rooks, Understanding of hydrogen silsesquioxane electron resist for sub-5-nm-half-pitch lithography. J. Vac. Sci. Technol. B **27**(6), 2622–2627 (2009)
44. W. Chao, B.D. Harteneck, J.A. Liddle, E.H. Anderson. D.T. Attwood, Soft x-ray microscopy at a spatial resolution better than 15 nm. Nature **435**(7046), 1210–1213 (2005)
45. Y. Usami, T. Watanabe, Y. Kanazawa, K. Taga, H. Kawai, K. Ichikawa, 405 nm laser thermal lithography of 40 nm pattern using super resolution organic resist material. Appl. Phys. Express **2**, 126502 (2009)
46. L. Li, R.R. Gattass, E. Gershgoren, H. Hwang, J.T. Fourkas, Achieving l/20 resolution by one-color initiation and deactivation of polymerization. Science **324**, 910–913 (2009)
47. Y. Cao, M. Gu, λ/26 silver nanodots fabricated by direct laser writing through highly sensitive two-photon photoreduction. Appl. Phys. Lett. **103**, 213104 (2013)
48. Z. Gan, Y. Cao, R.A. Evans, M, Gu, Three-dimensional deep sub-diffraction optical beam lithography with 9 nm feature size. Nat. Commun. **4**, 2061 (2013)
49. S.Y. Chou, P.R. Krauss, P.J. Renstrom, Imprint of sub-25 nm vias and trenches in polymers. Appl. Phys. Lett. **67**, 3114 (1995)
50. http://www.itrs.net/. Accessed 2017

51. J.V. Schoot, H. Schift, Next-generation lithography-an outlook on EUV projection and nanoimprint. Adv. Opt. Techn. **6**(3–4), 159–162 (2017)
52. M.T. Gale, C. Gimkiewicz, S. Obi, M. Schnieper, J. Sochtig, H. Thiele, S. Westenhofer, Replication technology for optical microsystems. Opt. Lasers Eng. **43**, 373–386 (2005)
53. M. Colburn, S. Johnson, M. Stewart, S. Damle, T. Bailey, B. Choi, M. Wedlake, T. Michaelson, S.V. Sreenivasan, J. Ekerdt, C.G. Willson, Step and flash imprint lithography: a new approach to high-resolution patterning. Proc. SPIE **3676**, 379–385 (1999)